Title: Theoretical validation of growth curves for quantifying phage-bacteria interactions

Authors: Michael Blazanin[1,2,3], Emma Vasen[1], Cèlia Vilaró Jolis[4], William An[1], Paul E. Turner[1,2,3,5]

[1]Department of Ecology and Evolutionary Biology, Yale University, New Haven, Connecticut, USA

[2]Center for Phage Biology & Therapy, Yale University, New Haven, Connecticut, USA

[3]Quantitative Biology Institute, Yale University, New Haven, Connecticut, USA

[4]Department of Biochemistry, Universitat de Barcelona, Barcelona, Spain

[5]Program in Microbiology, Yale School of Medicine, New Haven, Connecticut, USA

Correspondence:

Preprint:

Classification: Biological Sciences > Microbiology

Keywords:

Abstract

Bacteria-infecting viruses, bacteriophages, are the most abundant biological entities on the planet, frequently serving as model systems in basic research and increasingly relevant for medical applications such as phage therapy. A common need is to quantify the infectivity of a phage to a given bacterial host (or the resistance of a host to a phage). However, current methods to quantify infectivity suffer from low-throughput or low-precision. One method that has the potential for high-throughput and high-precision quantification of phage-bacteria interactions is growth curves, where bacterial density is measured over time in the presence and absence of phages. Recent work has proposed several approaches to quantify these curves into a metric of phage infectivity. However, little is known about how these metrics relate to one another or to underlying phage and bacterial traits. To address this gap, we apply ecological modeling of phage and bacterial populations to simulate growth curves across a wide range of trait values. Our findings show that many growth curve metrics provide parallel measures of phage infectivity. Informative metrics include the peak and decline portions of bacterial growth curves, are driven by the interactions between underlying phage and bacterial traits, and correlate with conventional measures of phage fitness. Moreover, we show how intrapopulation trait variation can alter growth curve dynamics. Finally, we test the sensitivity of growth curve metrics to inoculum densities, and assess techniques to compare growth curves across different bacterial hosts. In all, our findings support the use of growth curves for precise high-throughput quantification of phage-bacteria interactions across the microbial sciences.

Significance

Bacteriophages are viruses that infect bacteria. Phages have long been laboratory models and are increasingly being explored as antimicrobials. Commonly, we need to quantify how well a phage infects a bacterial strain. Unfortunately, current methods are either laborious or imprecise. One method that could be better is growth curves, where bacterial growth is measured over time in the presence or absence of phages. However, it has remained unclear how to use such data to produce a single metric of phage infectivity. Here, we used simulations to show that many different metrics provide parallel measures of phage infectivity that match conventional measures across a range of conditions. Our work suggests that growth curves can provide rapid, precise measurement of phage infectivity.

Introduction

Bacteriophages are the most abundant and diverse biological entities on the planet (1–4). Not only do phages play key roles in global ecosystem functioning, they have long been used as laboratory models in molecular biology, ecology, and evolutionary biology, and are increasingly relevant for medical application as phage therapy (5). Phages depend on bacterial host cells, hijacking cellular machinery to replicate their genetic material and produce new virion particles. However, phages can vary immensely in their success at infecting and replicating in a given host cell. This can be driven both by variation in phage adaptation to infect and replicate in a given host, as well as variation in bacterial adaptation to resist phage infection and replication via numerous defense mechanisms (6, 7).

Because of this variation, a common need is to quantify the infectivity of a phage on a given bacterial host (reciprocally, the resistance of a bacterial host to a given phage). Current approaches to quantify phage infectivity (and bacterial resistance) exhibit tradeoffs between throughput and precision (8, 9). Specifically, some approaches (e.g. the efficiency-of-plaquing assay (10–12)) provide low-throughput but high-precision measures of phage infectivity, while other approaches (e.g. cross-streaks and spot-tests (13)) provide high-throughput but low-precision measures of infectivity, often only providing a binary measure of infectivity. Moreover, none of these approaches can be easily automated, for instance with assays conducted by liquid-handling robots.

One method that has the potential for scalable high-throughput quantification is growth curves of bacteria in the presence of phages. Growth curves are collected by growing bacteria in an automated spectrophotometer, which obtains measures that are proxies for bacterial cell densities (e.g., light-scattering/optical density) at defined time intervals. By collecting growth curves of bacteria cultured in the presence of phages, once can observe the effect of phages on the population density of bacteria over time. Indeed, growth curves are a widely-used assay of phage-bacteria interactions, often to measure the infectivity of phages on bacterial strains (14–41).

Recent work has proposed a number of metrics that can be calculated from growth curve data as quantitative measures of phage infectivity. Some approaches focus on specific portions of the growth curve data (Fig 1), including maximum density, area under the curve (AUC), or extinction time (42–50). Other proposals use multivariate analyses like principal component analysis to produce summary metrics (23, 51). However, little is known about how these metrics relate to one another, how they vary depending on underlying phage and bacterial traits, and how they relate to conventional measures of phage infectivity.

To address this knowledge gap, we leverage an approach from another body of literature: the ecological modeling of phage-bacteria communities. There has been extensive theoretical work on phage-bacteria interactions (52, 53), but little theoretical work has applied ecological modeling to understand how growth curves can be used to quantify phage infectivity (49). Moreover, direct implications of existing theoretical work for growth curve applications are limited, since theoretical work often focuses on long-term equilibria while experimental growth curve analyses use short-term dynamics.

Here, we bridge this gap between the two fields, using ecological modeling of population dynamics to inform applications of growth curves to quantify phage-bacteria interactions. We used common modeling approaches of susceptible bacteria, infected bacteria, phages, and nutrients to simulate growth curves of a single bacteria population and a single phage population with varying traits (Fig 1).

For instance, we manipulated traits like infection rate, phage burst size (number phages produced per infected cell), phage lysis time (the duration of time between host infection and lysis, when viral progeny are released), bacterial growth rate, and bacterial carrying capacity. We then applied proposed growth curve analysis metrics to these simulated data. Our findings show that many metrics provide parallel measures of phage infectivity, and that metrics often quantify generalized phage fitness. We also highlight the limitations of growth curve analyses in cases where bacterial resistance to phages arises and when comparing phages across different bacterial hosts.

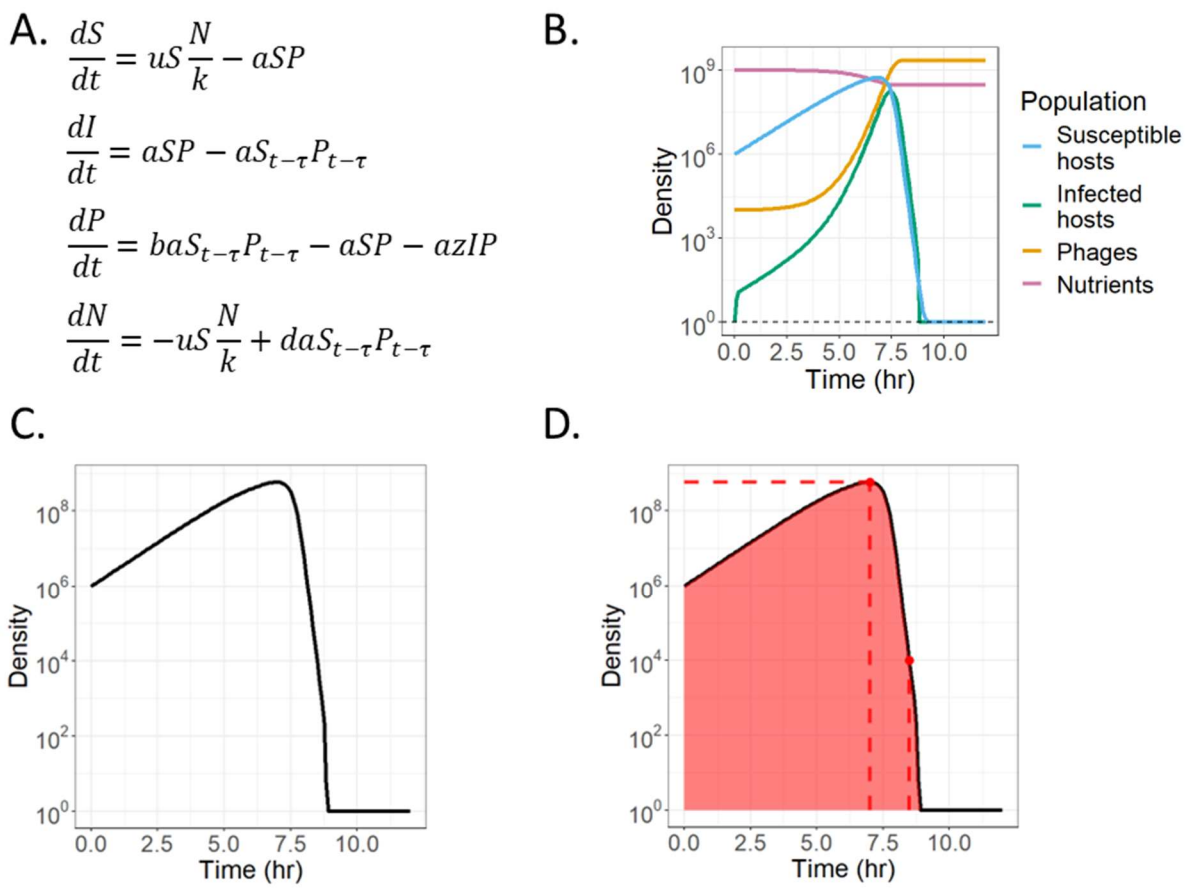

Fig 1. Simulating phage-bacteria growth curves. A. A modified SI-type system of delay differential equations was used to model the growth of bacterial and phage populations during growth curves. Susceptible bacteria (*S*) grow logistically (at rate *u*) up to a carrying capacity (*k*). Phage virions (*P*) infect susceptible hosts (at a rate *a*) and after a discrete lysis time (τ) release progeny virus particles (*b* per infection). Phages can also superinfect cells (at a rate *z*, relative to *a*). Lysis of cells releases nutrients back into the environment (at rate *d*). **B.** Simulation of this model shows initial growth of phage population and susceptible and infected bacterial populations, before bacteria go extinct and phage growth ceases. **C.** Experimentally, the typical available data output is the total bacterial population (*S* + *I*), plotted here. **D.** Metrics of the total bacterial population can then be extracted for comparison of different phages infecting bacteria, including peak density, peak time, time when density drops below a threshold ('extinction' time), and area under the curve (AUC).

Materials and Methods

Model implementation

We built a delay differential model of bacterial and phage growth (54) (Eqs. 1 – 4). Our model explicitly tracks the density of four populations through time: susceptible bacteria (S), infected bacteria (I), free phage particles (P), and nutrients (N). Note that we defined N to be in the same units as S and I, such that consumption of one unit of nutrients produces one susceptible cell. Moreover, when d = 1, the model of bacterial growth reduces to logistic growth. For convenience, we let k be the carrying capacity of cells, and define $k = S_0 + I_0 + N_0$. All populations without a subscript are assumed to be the current value at time t. Description of all parameters and the default value used in our simulations are provided in Table 1.

$$\frac{dS}{dt} = uS\frac{N}{k} - aSP \quad [1]$$

$$\frac{dI}{dt} = aSP - aS_{t-\tau}P_{t-\tau} \quad [2]$$

$$\frac{dP}{dt} = -aSP + baS_{t-\tau}P_{t-\tau} - azIP \quad [3]$$

$$\frac{dN}{dt} = -uS\frac{N}{k} + daS_{t-\tau}P_{t-\tau} \quad [4]$$

This model produces growth curves under the assumption of no plasticity in any traits. However, susceptibility to phage infection is known to decline as bacterial growth slows and bacteria enter stationary phase (52, 55–59). To identify simulated growth curves where this assumption is most likely to be violated, we identified growth curves which approximately reached their carrying capacity if $S + I \geq 0.9 * k$ at any point in time. In some plots in the main text these simulations are excluded (as noted in the figure legends), but plots with all simulations are included in the supplement.

Modeling variation in susceptibility to infection

To explicitly model variation in the susceptibility of bacteria to phage infection, we implemented two previously-published approaches (52). In the first, we modeled decreasing phage growth as nutrient density and bacterial growth rate decline via changes in the infection rate (60), burst size (57, 60, 61), and lysis time (26, 52, 62) (see Supplemental Results). In the second, we modeled transitions to a resistant nongrowing sub-population of cells (63) (Eqs. 5 – 6) (See Supplemental Results for models where the resistant sub-population of cells has non-zero growth, and where transitions from S to R are non-linear). Description of all parameters and the default value used in our simulations are provided in Table 1.

$$\frac{dS}{dt} = u_S S\frac{N}{k} - a_t SP - hu_S S \quad [5]$$

$$\frac{dR}{dt} = hu_S S \quad [6]$$

Table 1. Model parameter terms, their definitions, and the value used for simulations except when noted otherwise.

Parameter	Definition	Default Value
u	Maximum per-capita growth rate of susceptible cells	0.0179/min (doubling time of ~39 minutes)
k	Carrying capacity of cells	10^9 CFU/mL
a	Maximum infection rate of susceptible cells by free phage particles	10^{-10} infections/cell/phage
b	Burst size: number of phages produced by each infected cell	50 phages/cell
τ	Lysis time, the lag between infection of susceptible cell and lysis to release new phages	31.6 minutes
z	Scaling parameter for rate of superinfection of infected cells by free phages relative to rate of infection of susceptible cells	1
d	Fraction of nutrients replenished by each cell death	0
h	Transition rate of susceptible cells to resistant cells, relative to growth rate	0

Data availability

Data was generated using deSolve (64) and analyzed using gcplyr (65) in R v4.2.2. All code used to generate, analyze, and visualize data is available at https://github.com/mikeblazanin/growth-curves.

Results

We first sought to test how the various different growth curve metrics relate to one another, since it remains unclear whether, and to what degree, different metrics are correlated. To do so, we simulated growth curves using phages with a wide array of trait values and calculated metrics for each growth curve. Across all curves, bacterial density increases, peaks, then declines to extinction. Perhaps unsurprisingly, we find that growth curve metrics are tightly correlated with one another (Figs 2, S1). For instance, there is a close relationship between the peak density of the bacterial population (peak density) and the time when that peak occurs (peak time) (Figs 2A, S1A). Similarly, peak time and area under the curve (AUC) are closely related (Figs 2B, S1B). In addition, peak time is approximately linearly related to the time when bacterial density drops below some threshold density ('extinction' time) (Figs 2C, S1C, S2). These patterns are robust to changes in bacterial traits (Fig S3). These findings suggest that changes in phage traits largely alter growth curve metrics along a single axis of variation, and that different growth curve metrics provide parallel measures of phage infectivity.

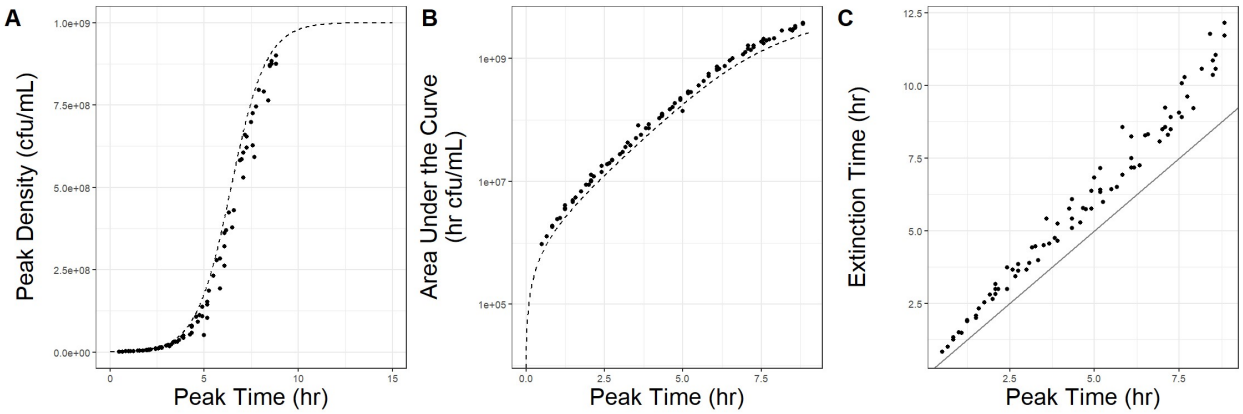

Fig 2. Phage-bacteria growth curve characteristics are tightly related to each other. Phage-bacteria growth curves were simulated with varying infection rates (10^{-12}, 10^{-11}, 10^{-10}, 10^{-9}, 10^{-8} /CFU/PFU/min), lysis times (10, 17.8, 31.6, 56.2, 100 mins), and burst sizes (5, 15.8, 50, 158, 500 PFU/infection). For each curve, the density and time when bacterial density peaked, area under the bacterial density curve, and time when bacterial density dropped below 10^4 CFU/mL (extinction time) were calculated. Each simulation is plotted as a single point, with growth curves where bacteria approximately reached their carrying capacity not plotted here (see Fig S1). **A.** For reference, the density of bacteria growing in the absence of phages up to peak time is plotted as a dashed line. **B.** For reference, area under the curve of bacteria growing in the absence of phages up to peak time is plotted as a dashed line. **C.** For reference, the 1:1 line is plotted.

Given the observed relationships between growth curve metrics, we sought to understand whether different portions of growth curve data are more or less informative for quantifying phage infectivity. When examining growth curves simulated with phages varying in their infection rates, we observed that the incline portion of the density dynamics is unaffected by infection rate (Fig 3A), or burst size or lysis time (Fig S4). This suggests that phage infectivity generally does not alter bacterial population dynamics during the incline portion of the data. In contrast, the slope of the decline portion of the density dynamics is strongly correlated with the peak bacterial density (Figs 3B, S5). Thus, growth curve analyses should largely disregard the incline portion of the data, focusing on the more-informative peak and decline portions of the data for quantifying phage infectivity.

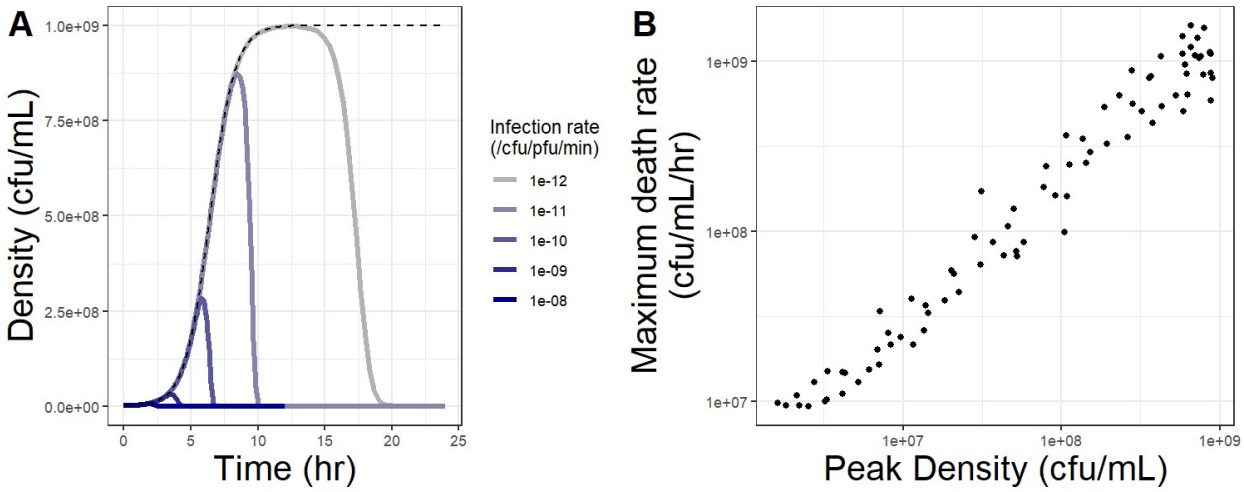

Fig 3. Information encoded in the incline, peak, and decline portions of phage-bacteria growth curve dynamics. A. Incline portion of growth curve dynamics provide no information about phage infectivity. Phage-bacteria growth curves were simulated with varying infection rates, plotting the total bacterial density over time. The dashed line denotes bacterial growth in the absence of phages. **B.** Peak and decline portion of growth curve dynamics provides parallel information. Phage-bacteria growth curves were simulated with varying infection rates (10^{-12}, 10^{-11}, 10^{-10}, 10^{-9}, 10^{-8} /CFU/PFU/min), lysis times (10, 17.8, 31.6, 56.2, 100 mins), and burst sizes (5, 15.8, 50, 158, 500 PFU/infection). For each curve, the peak bacterial density and the maximum downward slope during bacterial population decline are plotted. Growth curves where bacteria approximately reached their carrying capacity are not plotted here (see Fig S5)

We next sought to understand how growth curve metrics are related to the underlying phage and bacterial traits included in our model. In particular, it is unclear which traits have effects on growth curve metrics, and whether and how contributing traits interact with one another in determining the resulting metrics. To answer those questions, we simulated growth curves with phages with infection rates and lysis times along a grid of values, then calculated the peak time (of bacterial density) for each simulation. When plotted as a surface, we see that peak time is affected by both infection rate and lysis time (Fig 4). Moreover, infection rate and lysis time interact to produce a concave landscape, jointly determining peak time. Similar patterns are found for other phage (Fig S6) and bacterial (Fig S7) traits in the model, as well as when considering other growth curve metrics (Figs S8, S9, S10). In all, these data show that growth curve metrics are determined by the interactions between all phage and bacterial traits, suggesting that growth curve metrics can act as a generalized measure of phage fitness.

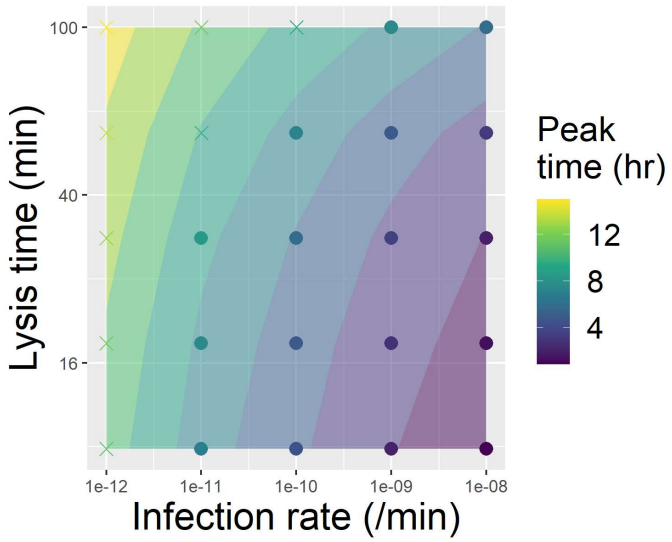

Fig 4. Phage-bacteria growth curve characteristics are driven by interactions between traits. Phage-bacteria growth curves were simulated with varying infection rates and lysis times, plotting the time when bacterial densities peaked. Each point is a single simulation, with linear interpolation of the surface between points for visualization. Growth curves where bacteria approximately reached their carrying capacity are plotted as an "X" here.

Given that growth curve metrics are tightly related to one another and driven by the interaction of bacterial and phage traits, we sought to understand how growth curve metrics relate to traditional measures of phage fitness. For instance, one common measure of phage fitness is the growth of the *phage* population over time. Indeed, past work has shown that the average phage growth rate during a growth curve has a negative relationship with bacterial extinction time both *in vitro* and *in silico* (49). We simulated growth curves using phages with a wide array of trait values, observing that our model reproduces this pattern (Figs 5A, S11A). Moreover, we now show how this relationship arises (Fig 5B, S11B). Specifically, the final phage density is largely equal to the product of the phage's burst size and the peak bacterial density: once all the bacteria present at the peak are converted into phages, they comprise the bulk of the phages present at the end of the growth curve. At small burst sizes, this pattern is noisy; as burst size increases, it increasingly dominates the effect on final phage density, and the pattern becomes stronger. These findings suggest that the extinction time metric, and by extension all the other closely-related metrics (Fig 2), are correlated with conventional measures of phage fitness.

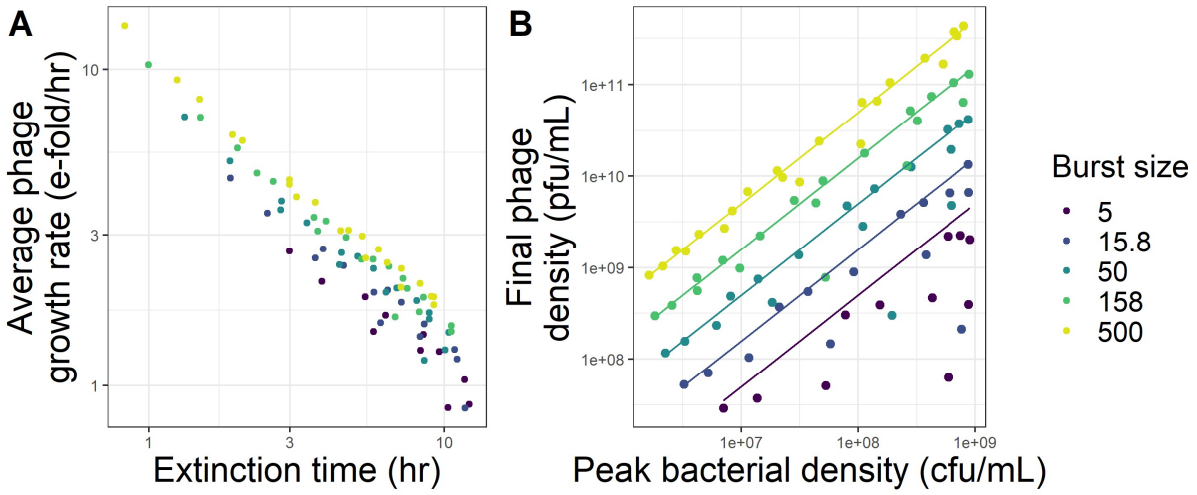

Fig 5. Phage-bacteria growth curve metrics relate to conventional measures of phage fitness. Phage-bacteria growth curves were simulated with varying infection rates (10^{-12}, 10^{-11}, 10^{-10}, 10^{-9}, 10^{-8} /CFU/PFU/min), lysis times (10, 17.8, 31.6, 56.2, 100 mins), and burst sizes (5, 15.8, 50, 158, 500 PFU/infection). For each curve, the peak bacterial density, time when bacterial density dropped below 10^4 CFU/mL (extinction time), and final phage density were calculated. Each simulation is plotted as a single point, with growth curves where bacteria approximately reached their carrying capacity not plotted here (see Fig S11). **A.** The average growth rate of phages during each simulated growth curve was calculated as $\frac{\log(P_{final}/P_0)}{t_{final}}$ using the extinction time as the final timepoint. **B.** Lines show the predicted relationship $P_{final} = b * (S_{peak} + I_{peak})$, where b is the burst size and S+I is the total bacterial density.

We next sought to understand how relaxation of a key assumption of our model would alter growth curve dynamics. Thus far, our models were constructed under the assumption that bacterial susceptibility to phages is constant, both over time and within the bacterial population. Under such an assumption, the inevitable outcome of a phage-bacteria growth curve is bacterial extinction (Table S1). However, this assumption is unlikely to be realistic. *In vitro* bacterial susceptibility often declines as bacterial growth slows (52, 55–59), and experimental growth curves often exhibit incomplete lysis of bacterial populations that cannot be generated by our simple model ((14), Fig S12). To assess the effects of relaxing this assumption, we used the two frequently-published approaches to incorporate variation in host susceptibility into our model (52). First, we modeled phage growth weakening as nutrients become scarce and bacterial growth slows (26, 52, 57, 60–62). Under these conditions, we find that bacterial populations can avoid extinction if they deplete nutrients sufficiently that phage infectivity becomes zero (Table S1). However, under none of these conditions are bacterial populations observed to experience partial lysis (Figs S14, S15, S16). Second, we introduced subpopulations of bacteria that vary in their susceptibility to phage infection to approximate intrapopulation variation (63). Under conditions where one sub-population is completely resistant to phage infection, the bacterial population avoids extinction by persisting in the resistant sub-population (Table S1). Moreover, transitions to a resistant sub-population can reproduce empirically-observed patterns of partial lysis of bacterial populations (Figs 6, S17, S18). These results suggest that slowing phage growth as bacterial growth

slows can alter growth curve dynamics, but that partial lysis patterns are likely explained by the presence of sub-populations of bacteria with varying susceptibility to phage infection.

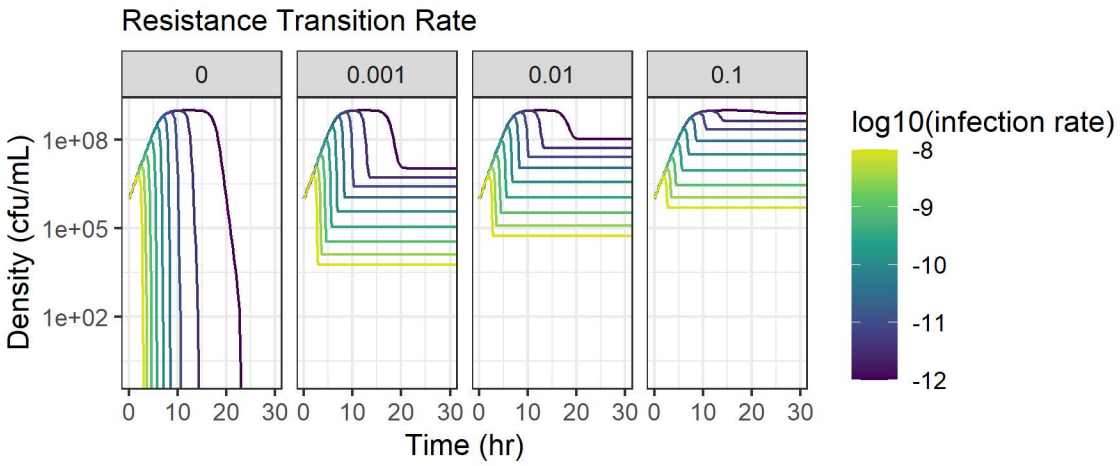

Fig 6. Cellular transitions into resistant subpopulation can reproduce partial population lysis in phage-bacteria growth curves. Growth curves were simulated with varying infection rates and varying constant rates of transition to resistance. Resistance transition rates are expressed relative to the maximum cell growth rate.

Next, we set out to assess the sensitivities of growth curve metrics to the inoculum densities of bacteria or phages. We simulated growth curves with varying initial densities of bacteria or phages. We then compared how strongly growth curve metrics were affected by initial densities versus phage infectivity. We found that changes in the initial density of bacteria or phages can strongly alter growth curve metrics on the same order of magnitude as changes in infectivity (Figs 7, S19, S20, S21, S22). Thus, normalization of initial bacterial and phage densities is likely to be necessary when preparing a growth curve assay. In practice, this normalization can be subject to stochastic noise, where the true initial densities differ from the intended initial densities. Fortunately, the extent of this noise is minimal, and is only likely to obscure small differences in phage infectivity (Fig S23, S24, S25).

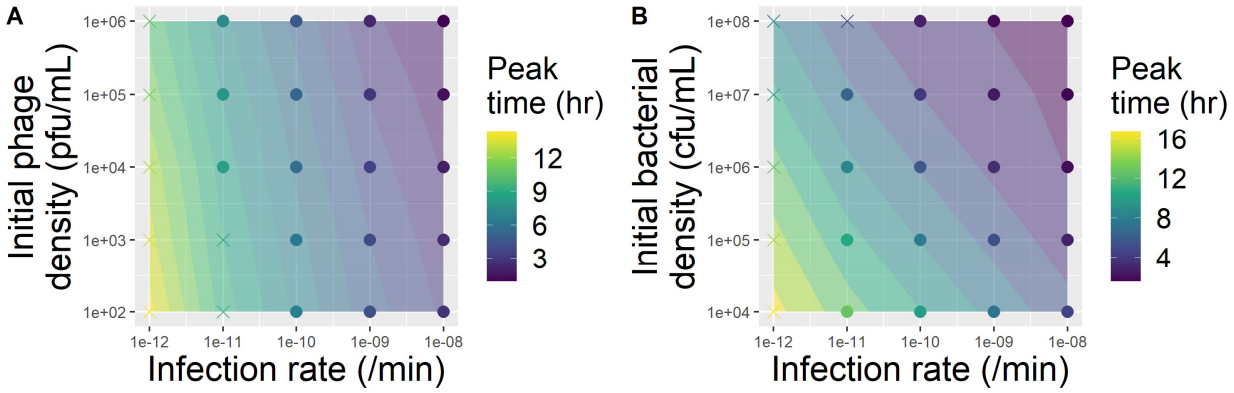

Fig 7. Inoculum densities alter growth curve metrics. Phage-bacteria growth curves were simulated with varying infection rates and initial bacterial (A) or phage (B) densities (while holding the other constant). Each point is a single simulation, with the time when the bacterial density peaked plotted as the color, and linear interpolation of the surface between points for visualization. Growth curves where bacteria approximately reached their carrying capacity are plotted as an "X" here. **A.** The initial density of phages was held constant at 10^4 PFU/mL. **B.** The initial density of bacteria was held constant at 10^6 CFU/mL.

Finally, we set out to test how to use growth curves to compare phage infectivity across different bacterial hosts. For instance, consider when different bacterial hosts vary in their susceptibility to a phage but also vary in their growth rate or carrying capacity. How can we eliminate the effects of differences in bacterial growth to infer differences in phage infectivity? One proposed approach is to use multivariate ordination methods like principal component analysis (PCA) to quantify phage infectivity (23, 51). We simulated growth curves of varying bacteria with a phage and applied PCA, but found that the PCA axes did not correlate with phage infectivity (Fig S26). An alternate proposed approach is to use area under the curve (AUC) normalized by dividing by the AUC of a phage-free control (44, 48, 50). We simulated growth curves of varying bacteria with a phage and found that AUC generally correlates well with phage infectivity. However, under some conditions normalizing can counterintuitively worsen the signal of phage infectivity (Figs 8, S27). Specifically, when bacteria vary in their carrying capacities, the AUC of the phage-free control varies *more* than the AUC of the phage-bacteria curves, so normalizing worsens the signal of infectivity (Fig 8A). In contrast, when bacteria vary in their growth rates, the AUC of the phage-free control varies less than the AUC of the phage-bacteria curves, so normalizing improves the signal of infectivity (Fig 8B). These results suggest that normalizing AUC should only be done when phage-bacteria AUC values are expected to vary more than the control bacteria-only AUC values.

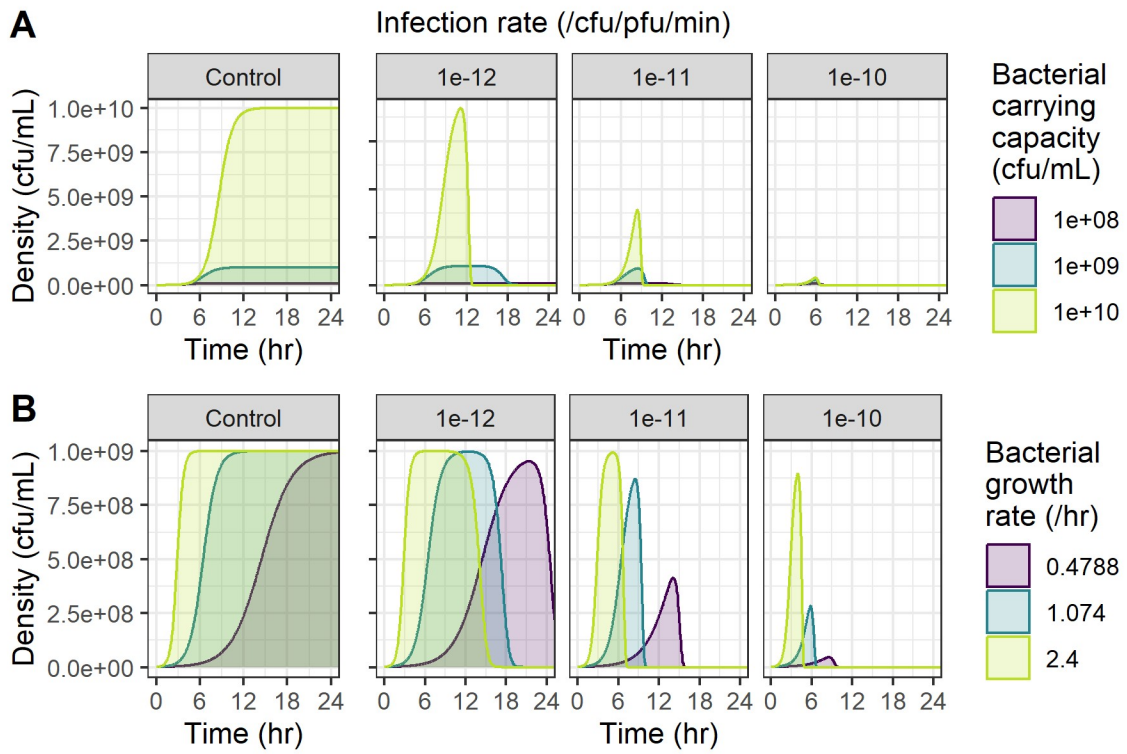

Fig 8. Normalizing area under the curve (AUC) can improve or worsen the signal of phage infectivity. Bacterial growth curves were simulated with varying carrying capacities (A), or varying growth rates (B), in the absence (Control) or presence of phages with different infection rates. **A.** When bacteria vary in their carrying capacity, the control AUC values vary more than the AUC values in the presence of phages, so normalizing will worsen the signal of phage infectivity. **B.** When bacteria vary in their growth rate, the control AUC values vary less than the AUC values in the presence of phages, so normalizing improves the signal of phage infectivity.

Discussion

Here, we set out to test how metrics of bacterial growth curves can be used to quantify phage infectivity and bacterial resistance. We found that many metrics of growth curves provide correlated information with each other on infectivity and resistance (Fig 2). Specifically, this information is provided in the peak and decline phases of the curves, whereas the initial growth phase is largely uninformative (Fig 3). We then showed that growth curve metrics act as an overall measure of phage fitness, incorporating effects from multiple phage and bacterial traits (Fig 4). Moreover, these metrics correlate with traditional measures of phage fitness (Fig 5). We tested how variation in infectivity can alter growth curve dynamics (Fig 6) and showed that growth curve metrics are largely robust to noise in initial conditions (Fig 7). Finally, we highlighted the limitations of proposed methods to compare infectivity and resistance across distinct bacterial hosts (Fig 8).

This work shows that growth curve metrics can be used to quantify general phage infectivity, but are unlikely to be useful to quantify specific phage life history traits like adsorption (cell-attachment) rate, burst size, or lysis time. We found no clear way to infer adsorption rate or lysis time from growth curve

metrics. In principle, it could be possible to measure phage density after a growth curve and combine that information with peak bacterial density to estimate burst size (Fig 5B). However, in practice, single step phage growth curves remain likely to give more precise and accurate measures of specific phage traits.

Some patterns from these new findings also align with the results of past work in other study systems. For instance, our simulations show that the initial phase of growth curve data provides little information about the infectivity of a phage (Fig 3A). Similar findings have been reported in the epidemiology literature, where the initial growth of an epidemic provides little indication of the eventual severity of the epidemic (66, 67). Additionally, our simulations recreated previously-reported patterns between phage growth rate and bacterial extinction time (Fig 5A). Indeed, our work expanded on these findings by showing how this pattern arises from an interaction between phage burst size and the peak of bacterial density (Fig 5B, S11B).

Using simulations, we were able to directly manipulate inoculation conditions and observe how they altered growth curve dynamics. However, in laboratory studies, normalizing phage inoculum densities can be difficult. Phages are commonly quantified by plaquing them on a bacterial host, but since phages vary in their plaquing efficiency across different hosts the true phage particle concentration may be far from the inferred concentration. Further work is necessary to improve on this shortcoming of plaque-based density estimation, perhaps exploring how alternate methods like qPCR or flow cytometry could be implemented for common-practice enumeration of phage density.

We showed that observed patterns of partial population lysis during growth curves (Fig S12) cannot be explained by declining phage infectivity as bacterial growth slows (Figs S14, S15, S16), but instead can be explained by subpopulations of bacteria that vary in their susceptibility to phage infection (Fig 6). Indeed, such mechanisms have previously been discovered and shown to underlie partial population lysis in some experimental growth curves (14). However, it remains unclear how to interpret partial lysis patterns with respect to phage susceptibility. Bacterial density after partial population lysis is driven not only by the phage infection rate, but also by the transition rate from susceptibility to resistance (Fig 6). Further work is needed to understand how these two traits are related to one another before a clear interpretation can be drawn from the density after partial population lysis.

Our work has established a broad foundation for using phage-bacteria growth curves to quantify phage infectivity and bacterial resistance, opening many avenues for future work. Given the limited theoretical work on phage-bacteria growth curves (this paper and (49)), future theoretical work could explore the effects of numerous biological phenomena, including stochasticity, coinfection exclusion, cooperation, failed infections, continuous intrapopulation trait variation, or lysogeny (phage integration into the host bacterial chromosome). Additionally, theoretical work could explore alternate uses of growth curves than quantifying phage infectivity, like quantifying the evolution of bacterial resistance to phage infection. At the same time, further empirical is needed. For instance, to understand the relationship between cell density and the measured proxies of cell density (e.g., optical density) (68–70), and to test theoretical predictions with phages whose life history traits have been experimentally quantified *a priori*.

In all, we have shown that measuring growth curves can be a powerful approach for quantifying phage-bacteria interactions. Growth curves complement existing methods for measuring phage infectivity. They occur in liquid culture, which may better reflect the interactions of phages and bacteria in liquid

(planktonic) environments than agar surface-based assays of infectivity. Moreover, growth curves are highly scalable, able to be collected in parallel for many replicates at once and easily implemented by automated platforms. Given that growth curves are already widely used heuristically in the phage-bacteria literature, our findings suggest that they may be ripe for quantitative application from basic to applied questions.

Acknowledgements

Thanks to Alita Burmeister, Tiffany Hamidjaja, Catherine Hernandez, Jordan Lewis, and Albert Vill for feedback on the manuscript. Thanks to members of the Turner lab for feedback on the work in this project. Thanks to Teresa Carter for contributions to very early work on this project. Thanks to the Yale Institute for Biospheric Studies for funding supporting this work. Thanks to the Yale STARS program for funding supporting WA during this project.

References

1. A. R. Mushegian, Are there 10^31 virus particles on Earth, or more, or less? *Journal of Bacteriology* **202**, e00052-20 (2020).

2. W. H. Pope, *et al.*, Whole genome comparison of a large collection of mycobacteriophages reveals a continuum of phage genetic diversity. *eLife* **4**, e06416 (2015).

3. F. Rohwer, Global phage diversity. *Cell* **113**, 141 (2003).

4. J. C. Ignacio-Espinoza, S. A. Solonenko, M. B. Sullivan, The global virome: not as big as we thought? *Current Opinion in Virology* **3**, 566–571 (2013).

5. K. E. Kortright, B. K. Chan, J. L. Koff, P. E. Turner, Phage Therapy: A Renewed Approach to Combat Antibiotic-Resistant Bacteria. *Cell Host and Microbe* **25**, 219–232 (2019).

6. H. G. Hampton, B. N. J. Watson, P. C. Fineran, The arms race between bacteria and their phage foes. *Nature* **577**, 327–336 (2020).

7. J. Antonovics, *et al.*, The origin of specificity by means of natural selection: Evolved and nonhost resistance in host-pathogen interactions. *Evolution* **67**, 1–9 (2013).

8. T. Jagdish, A. N. Nguyen Ba, Microbial experimental evolution in a massively multiplexed and high-throughput era. *Current Opinion in Genetics & Development* **75**, 101943 (2022).

9. T. Glonti, J.-P. Pirnay, In Vitro Techniques and Measurements of Phage Characteristics That Are Important for Phage Therapy Success. *Viruses* **14**, 1490 (2022).

10. E. Kutter, "Phage Host Range and Efficiency of Plating" in *Bacteriophages: Methods and Protocols, Volume 1: Isolation, Characterization, and Interactions*, Methods in Molecular Biology™., M. R. J. Clokie, A. M. Kropinski, Eds. (Humana Press, 2009), pp. 141–149.

11. A. M. Kropinski, A. Mazzocco, T. E. Waddell, E. Lingohr, R. P. Johnson, "Enumeration of Bacteriophages by Double Agar Overlay Plaque Assay" in *Bacteriophages: Methods and Protocols, Volume 1: Isolation, Characterization, and Interactions*, Methods in Molecular Biology™., M. R. J. Clokie, A. M. Kropinski, Eds. (Humana Press, 2009), pp. 69–76.

12. A. Mazzocco, T. E. Waddell, E. Lingohr, R. P. Johnson, "Enumeration of Bacteriophages by the Direct Plating Plaque Assay" in *Bacteriophages: Methods and Protocols, Volume 1: Isolation, Characterization, and Interactions*, Methods in Molecular Biology™., M. R. J. Clokie, A. M. Kropinski, Eds. (Humana Press, 2009), pp. 77–80.

13. A. Mazzocco, T. E. Waddell, E. Lingohr, R. P. Johnson, "Enumeration of Bacteriophages Using the Small Drop Plaque Assay System" in *Bacteriophages: Methods and Protocols, Volume 1: Isolation, Characterization, and Interactions*, Methods in Molecular Biology™., M. R. J. Clokie, A. M. Kropinski, Eds. (Humana Press, 2009), pp. 81–85.

14. J. C. Wohlfarth, *et al.*, L-form conversion in Gram-positive bacteria enables escape from phage infection. *Nat Microbiol* **8**, 387–399 (2023).

15. Z. Yu, *et al.*, Modeling multiphage-bacteria kinetics to predict phage therapy potency and longevity. bioRxiv [Preprint] (2022) https://www.biorxiv.org/content/10.1101/2022.11.11.516137v1 (accessed July 26, 2023).

16. C. N. Vassallo, C. R. Doering, M. L. Littlehale, G. I. C. Teodoro, M. T. Laub, A functional selection reveals previously undetected anti-phage defence systems in the E. coli pangenome. *Nat Microbiol* **7**, 1568–1579 (2022).

17. L. Tian, *et al.*, Self-assembling nanofibrous bacteriophage microgels as sprayable antimicrobials targeting multidrug-resistant bacteria. *Nat Commun* **13**, 7158 (2022).

18. J. H. Doss, N. Barekzi, D. T. Gauthier, Improving high-throughput techniques for bacteriophage discovery in multi-well plates. *Journal of Microbiological Methods* **200**, 106542 (2022).

19. M. E. K. Haines, *et al.*, Analysis of Selection Methods to Develop Novel Phage Therapy Cocktails Against Antimicrobial Resistant Clinical Isolates of Bacteria. *Frontiers in Microbiology* **12** (2021).

20. D. Gelman, *et al.*, Clinical Phage Microbiology: a suggested framework and recommendations for the in-vitro matching steps of phage therapy. *The Lancet Microbe* **2**, e555–e563 (2021).

21. K. M. Danis-Wlodarczyk, *et al.*, Friends or Foes? Rapid Determination of Dissimilar Colistin and Ciprofloxacin Antagonism of Pseudomonas aeruginosa Phages. *Pharmaceuticals* **14**, 1162 (2021).

22. E. J. Cano, *et al.*, Phage Therapy for Limb-threatening Prosthetic Knee Klebsiella pneumoniae Infection: Case Report and In Vitro Characterization of Anti-biofilm Activity. *Clinical Infectious Diseases* **73**, e144–e151 (2021).

23. J. M. Borin, S. Avrani, J. E. Barrick, K. L. Petrie, J. R. Meyer, Coevolutionary phage training leads to greater bacterial suppression and delays the evolution of phage resistance. *Proc. Natl. Acad. Sci. U.S.A.* **118**, e2104592118 (2021).

24. M. Benala, *et al.*, A revisited two-step microtiter plate assay: Optimization of in vitro multiplicity of infection (MOI) for Coliphage and Vibriophage. *Journal of Virological Methods* **294**, 114177 (2021).

25. D. Rajnovic, J. Mas, Fluorometric detection of phages in liquid media: Application to turbid samples. *Analytica Chimica Acta* **1111**, 23–30 (2020).

26. D. Ping, *et al.*, Hitchhiking, collapse, and contingency in phage infections of migrating bacterial populations. *ISME J* **14**, 2007–2018 (2020).

27. C. Gu Liu, *et al.*, Phage-Antibiotic Synergy Is Driven by a Unique Combination of Antibacterial Mechanism of Action and Stoichiometry. *mBio* **11**, e01462-20 (2020).

28. R. Nir-Paz, *et al.*, Successful Treatment of Antibiotic-resistant, Poly-microbial Bone Infection With Bacteriophages and Antibiotics Combination. *Clinical Infectious Diseases* **69**, 2015–2018 (2019).

29. Michael Habusha, Elhanan Tzipilevich, Osher Fiyaksel, Sigal Ben-Yehuda, A mutant bacteriophage evolved to infect resistant bacteria gained a broader host range. *Molecular Microbiology* **111**, 1463–1475 (2019).

30. C. A. Hernandez, B. Koskella, Phage resistance evolution in vitro is not reflective of in vivo outcome in a plant-bacteria-phage system. *Evolution* **73**, 2461–2475 (2019).

31. S. Aslam, *et al.*, Early clinical experience of bacteriophage therapy in 3 lung transplant recipients. *American Journal of Transplantation* **19**, 2631–2639 (2019).

32. F. Forti, *et al.*, Design of a Broad-Range Bacteriophage Cocktail That Reduces Pseudomonas aeruginosa Biofilms and Treats Acute Infections in Two Animal Models. *Antimicrobial Agents and Chemotherapy* **62**, e02573-17 (2018).

33. R. T. Schooley, *et al.*, Development and use of personalized bacteriophage-based therapeutic cocktails to treat a patient with a disseminated resistant Acinetobacter baumannii infection. *Antimicrobial Agents and Chemotherapy* **61**, e00954-17 (2017).

34. D. Cho, I. Lau, M. Li, D. Zhu, Development of a Microtiter Plate Assay for Real Time Analysis of T7 Bacteriophage Mediated Lysis of Escherichia coli. *Journal of Experimental Microbiology and Immunology* **21**, 6 (2017).

35. L. A. Estrella, *et al.*, Characterization of novel Staphylococcus aureus lytic phage and defining their combinatorial virulence using the OmniLog® system. *Bacteriophage* **6**, e1219440 (2016).

36. J. Bertozzi Silva, D. Sauvageau, Bacteriophages as antimicrobial agents against bacterial contaminants in yeast fermentation processes. *Biotechnol Biofuels* **7**, 123 (2014).

37. M. Henry, R. Lavigne, L. Debarbieux, Predicting in vivo efficacy of therapeutic bacteriophages used to treat pulmonary infections. *Antimicrobial Agents and Chemotherapy* **57**, 5961–5968 (2013).

38. I. N. Wang, Lysis timing and bacteriophage fitness. *Genetics* **172**, 17–26 (2006).

39. R. R. Raya, *et al.*, Isolation and Characterization of a New T-Even Bacteriophage, CEV1, and Determination of Its Potential To Reduce Escherichia coli O157:H7 Levels in Sheep. *Applied and Environmental Microbiology* **72**, 6405–6410 (2006).

40. S. T. Abedon, P. Hyman, C. Thomas, Experimental Examination of Bacteriophage Latent-Period Evolution as a Response to Bacterial Availability. *Applied and Environmental Microbiology* **69**, 7499–7506 (2003).

41. J. B. Lynch, B. D. Bennett, B. D. Merrill, E. G. Ruby, A. J. Hryckowian, Independent host- and bacterium-based determinants protect a model symbiosis from phage predation. *Cell Reports* **38** (2022).

42. R. M. Ceballos, C. L. Stacy, Quantifying relative virulence: when μ max fails and AUC alone just is not enough. *J Gen Virol* **102**, jgv001515 (2020).

43. C. J. Cooper, S. P. Denyer, J. Y. Maillard, Rapid and quantitative automated measurement of bacteriophage activity against cystic fibrosis isolates of Pseudomonas aeruginosa. *Journal of Applied Microbiology* **110**, 631–640 (2011).

44. M. Konopacki, B. Grygorcewicz, B. Dołęgowska, M. Kordas, R. Rakoczy, PhageScore: A simple method for comparative evaluation of bacteriophages lytic activity. *Biochemical Engineering Journal* **161**, 107652 (2020).

45. J.-Y. Maillard, T. s. Beggs, M. j. Day, R. a. Hudson, A. d. Russell, The use of an automated assay to assess phage survival after a biocidal treatment. *Journal of Applied Bacteriology* **80**, 605–610 (1996).

46. C. E. Martinez-Soto, *et al.*, PHIDA: A High Throughput Turbidimetric Data Analytic Tool to Compare Host Range Profiles of Bacteriophages Isolated Using Different Enrichment Methods. *Viruses* **13**, 2120 (2021).

47. D. Rajnovic, X. Muñoz-Berbel, J. Mas, Fast phage detection and quantification: An optical density-based approach. *PLOS ONE* **14**, e0216292 (2019).

48. Z. J. Storms, M. R. Teel, K. Mercurio, D. Sauvageau, The Virulence Index: A Metric for Quantitative Analysis of Phage Virulence. *PHAGE* **1**, 27–36 (2020).

49. P. E. Turner, J. A. Draghi, R. Wilpiszeski, High-throughput analysis of growth differences among phage strains. *Journal of Microbiological Methods* **88**, 117–121 (2012).

50. Y. Xie, L. Wahab, J. Gill, Development and Validation of a Microtiter Plate-Based Assay for Determination of Bacteriophage Host Range and Virulence. *Viruses* **10**, 189 (2018).

51. P. E. Sørensen, *et al.*, Classification of In Vitro Phage–Host Population Growth Dynamics. *Microorganisms* **9**, 2470 (2021).

52. C. Igler, Phenotypic flux: The role of physiology in explaining the conundrum of bacterial persistence amid phage attack. *Virus Evolution* **8**, veac086 (2022).

53. J. S. Weitz, *Quantitative Viral Ecology: Dynamics of Viruses and Their Microbial Hosts* (Princeton University Press, 2015).

54. B. R. Levin, F. M. Stewart, L. Chao, Resource-Limited Growth, Competition, and Predation: A Model and Experimental Studies with Bacteria and Bacteriophage. *The American Naturalist* **111**, 3–24 (1977).

55. B. Koskella, C. A. Hernandez, R. M. Wheatley, Understanding the Impacts of Bacteriophage Viruses: From Laboratory Evolution to Natural Ecosystems. *Annu. Rev. Virol.* **9**, 57–78 (2022).

56. M. Choua, J. A. Bonachela, Ecological and Evolutionary Consequences of Viral Plasticity. *The American Naturalist* **193**, 346–358 (2019).

57. D. Nabergoj, P. Modic, A. Podgornik, Effect of bacterial growth rate on bacteriophage population growth rate. *MicrobiologyOpen* **7**, e00558 (2018).

58. D. Bryan, A. El-Shibiny, Z. Hobbs, J. Porter, E. M. Kutter, Bacteriophage T4 Infection of Stationary Phase E. coli: Life after Log from a Phage Perspective. *Front. Microbiol.* **7** (2016).

59. H. Hadas, M. Einav, I. Fishov, A. Zaritsky, Bacteriophage T4 Development Depends on the Physiology of its Host Escherichia Coli. *Microbiology* **143**, 179–185 (1997).

60. S. J. Schrag, J. E. Mittler, Host-Parasite Coexistence: The Role of Spatial Refuges in Stabilizing Bacteria-Phage Interactions. *The American Naturalist* **148**, 348–377 (1996).

61. H. Schenk, M. Sieber, Bacteriophage can promote the emergence of physiologically sub-optimal host phenotypes. bioRxiv [Preprint] (2019) https://www.biorxiv.org/content/10.1101/621524v1 (accessed April 20, 2023).

62. A. L. Lloyd, Destabilization of epidemic models with the inclusion of realistic distributions of infectious periods. *Proceedings of the Royal Society of London. Series B: Biological Sciences* **267** (2001).

63. J. J. Bull, C. S. Vegge, M. Schmerer, W. N. Chaudhry, B. R. Levin, Phenotypic Resistance and the Dynamics of Bacterial Escape from Phage Control. *PLOS ONE* **9**, e94690 (2014).

64. K. Soetaert, T. Petzoldt, R. W. Setzer, Solving Differential Equations in R: Package deSolve. *Journal of Statistical Software* **33**, 1–25 (2010).

65. M. Blazanin, gcplyr: an R package for microbial growth curve data analysis. bioRxiv [Preprint] (2023) https://www.biorxiv.org/content/10.1101/2023.04.30.538883v1 (accessed April 30, 2023).

66. T. Sauer, *et al.*, Identifiability of Infection Model Parameters Early in an Epidemic. *SIAM J. Control Optim.* **60**, S27–S48 (2022).

67. O. Melikechi, *et al.*, Limits of epidemic prediction using SIR models. *J. Math. Biol.* **85**, 36 (2022).

68. J. A. Myers, B. S. Curtis, W. R. Curtis, Improving accuracy of cell and chromophore concentration measurements using optical density. *BMC Biophysics* **6**, 4 (2013).

69. J. Beal, *et al.*, Robust estimation of bacterial cell count from optical density. *Commun Biol* **3**, 1–29 (2020).

70. K. Stevenson, A. F. McVey, I. B. N. Clark, P. S. Swain, T. Pilizota, General calibration of microbial growth in microplate readers. *Sci Rep* **6**, 38828 (2016).

71. M. A. Brockhurst, A. D. Morgan, A. Fenton, A. Buckling, Experimental coevolution with bacteria and phage. The Pseudomonas fluorescens—Φ2 model system. *Infection, Genetics and Evolution* **7**, 547–552 (2007).

72. M. Blazanin, J. P. Moore, S. Olsen, M. Travisano, Fight not flight: parasites drive the bacterial evolution of resistance, not avoidance. bioRxiv [Preprint] (2023) https://www.biorxiv.org/content/10.1101/2023.04.29.538831v1 (accessed April 30, 2023).